Article

Optoelectronic Switching Memory Based on ZnO Nanoparticle/Polymer Nanocomposites

Ayoub H. Jaafar, Chris Lowe, Alex Gee, and Neil T. Kemp*

Cite This: https://doi.org/10.1021/acsapm.2c02034

Read Online

ACCESS | Metrics & More | Article Recommendations

ABSTRACT: Optoelectronic switching memories are emerging as practical candidates for applications of optically tunable neuromorphic computing systems and artificial vision systems. Here, we report on the fabrication of an optoelectronic switching memory device based on semiconducting zinc oxide nanoparticles (ZnO NPs) embedded within a photoactive azobenzene polymer. The device shows electronic resistive switching and a reversible optical switching effect upon changing the polarization of the applied light. Optical illumination with circularly/linearly polarized light expands/contracts the nanocomposite film and modifies the conduction pathway, facilitated by the presence of the ZnO NPs, as a semiconductor material within the insulating poly(disperse red 1 acrylate) material. The carrier transport and the operating switching mechanism are explained on the basis of the current−voltage ($I−V$) results. The reported device enables optical controllable resistive switching properties that may find applications in visual systems integrated within artificial intelligence networks.

KEYWORDS: resistive switching, optoelectronic, nanocomposite, azobenzene polymer, PDR1A, memristor
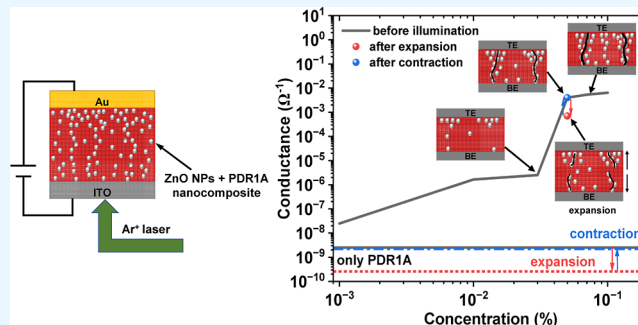
1. INTRODUCTION

Fabrication of optoelectronic switching memories is needed for future applications in artificial vision systems,[1,2] photonic integrated circuits,[3,4] neuromorphic computing systems,[5−7] light-switchable memory elements in optical communications,[8] and visual perception nervous systems.[9] This class of device enables not only the possibility to overcome the bottleneck limitations of traditional von Neumann computing architecture and the failing of Moore's law for scaling down architectures[4] but also offers significant memory properties such as low power consumption, high storage density, fast write/erase speeds, simple two terminal structure, and low complexity integrated circuits onto processor chips.[10−13]

Optoelectronic switching memories have been demonstrated in various materials such oxides,[3,10,12,14] 2D materials,[2,6,9] graphene oxide,[15] perovskites,[13] chalcogenides,[1] organics/polymers,[11,16,17] and organic−inorganic nanocomposites.[18−22] In particular, nanocomposites provide a number of advantages, including low cost, easy solution-based processing[23−25] *via* screen-printing or spin-coating, and easy tailoring of the materials' mechanical, electronic, and optical properties through chemical synthesis.[26−30] In comparison to inorganic material-based devices, nanocomposite-based resistive memories have demonstrated significant switching properties such as high ON/OFF ratios, ultra-low operating voltages, reduced power consumption, multilevel data storage, analogue switch-

ing, and flexibility.[31−35] However, the fabrication of organic−inorganic composites is still much less studied than devices having solely inorganic constituents.

In this work, we report on the fabrication of an optoelectronic switching memory that is fabricated by fast, low cost, and vacuum-free deposition methods. The device consists of semiconducting zinc oxide nanoparticles (ZnO NPs) embedded with an optically active polymer that is sandwiched between an indium tin oxide (ITO) bottom electrode and a Au top electrode. To control the device optically, we have used the azobenzene poly(disperse red 1 acrylate) (PDR1A) polymer which undergoes a reversible trans−cis photochemical isomerization upon optical excitation,[36] as shown in Figure 1c. Associated with this is a significant photomechanical response[37] caused by the progressive alignment of chromophores from repeated trans−cis−trans cycling, which occurs because of the overlap of the two absorption bands for the trans−cis and cis−trans transitions.[38,39] Circularly polarized light aligns the chromophores in
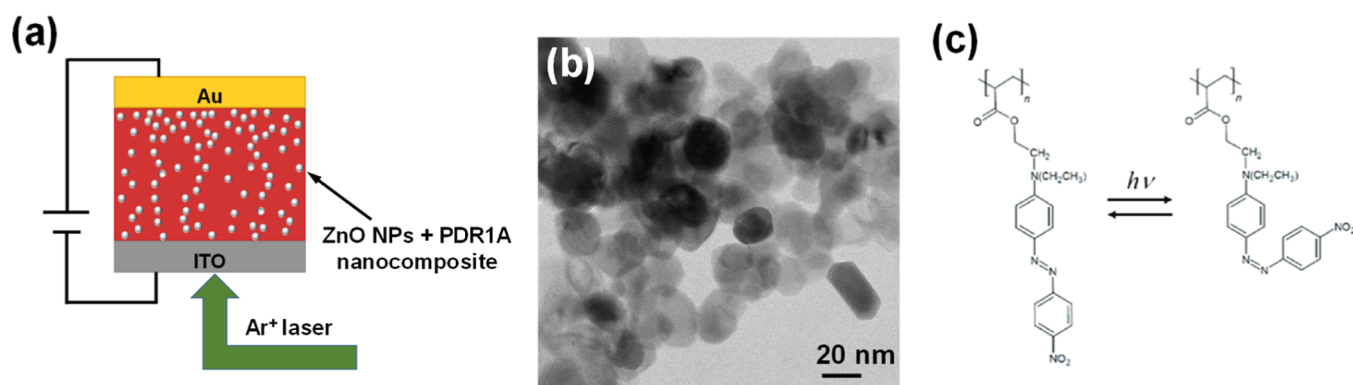
Figure 1. (a) Schematic of the optoelectronic switching memory consisting of ZnO NPs embedded within a thin film of PDR1A and deposited between ITO and Au electrodes. (b) TEM image of the ZnO NPs. (c) Trans−cis photochemical isomerization of the optically active azopolymer (PDR1A).
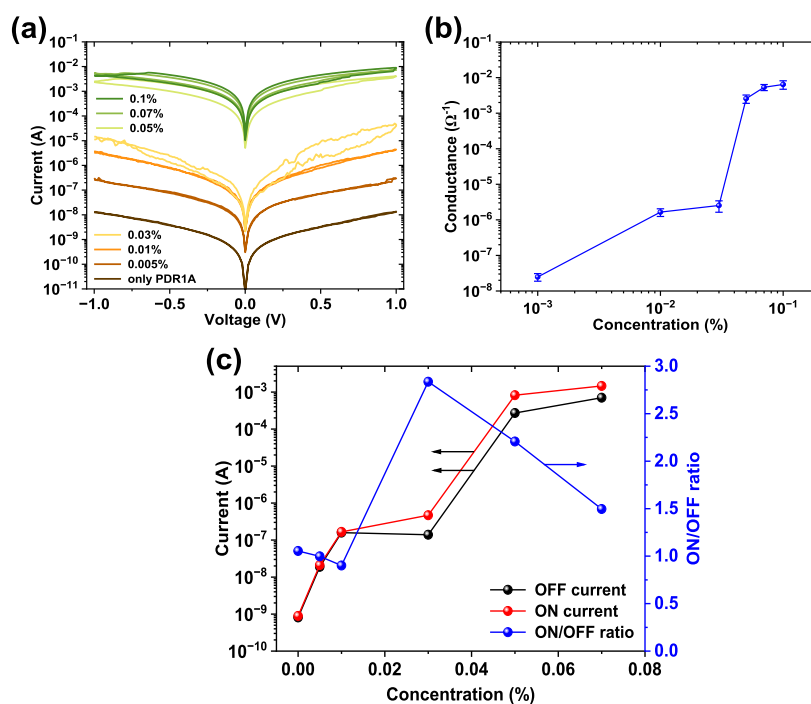

Figure 2. (a) Comparison of device characteristics for concentrations ranging from R_m = 0.0 (only PDR1A) to 0.1%, showing better stability and hysteresis in devices with $R_m \geq 0.05\%$ (b) Relationship between the concentration (R_m) of ZnO NPs and conductance in the low-voltage Ohmic region of the devices. (c) Plot of the ON/OFF ratio (left axis) and ON and OFF currents (@0.15 V) as a function of ZnO NP concentration (right axis).

the direction of the beam, causing the thickness of the film to increase, whereas linearly polarized light causes a reduction in film thickness when the beam is directed perpendicular to the surface, as reported previously.[19,22] Our group has previously reported memristor devices based on hybrid ZnO nanorods/PDR1A and nanocomposites such as gold (Au) NPs/PDR1A and TiO$_2$ nanorods/PDR1A. The devices showed both reversible electronic memristor switching and reversible polarization-dependent optical switching, the latter importantly enabling optical control of synaptic potentiation and depression, optical switching between short-term and long-term memory, and optical modulation of the synaptic efficacy *via* spike timing-dependent plasticity.[19,20,22] Altogether, the use of the PDR1A material for nanocomposite system-based electronic devices provides a unique functionality of optical control of memristor devices for neuromorphic network and

artificial intelligence applications. In this paper, the nanocomposite-based optoelectronic device demonstrates desirable memory properties such as a forming-free switching, low voltage operation, and importantly, optically tunable resistive switching properties based on the polarization properties of light. These properties are desirable for developing next-generation resistive switching memories for integrated photonic circuit applications.

2. EXPERIMENTAL SECTION

The resistive switching memory devices consist of a nanocomposite thin film (160 nm thick) made from the ZnO NPs and optically active azobenzene polymer (PDR1A) and sandwiched between ITO bottom and Au top electrodes (ITO/ZnO NPs−PDR1A/Au), as schematically shown in Figure 1a. PDR1A was purchased from Sigma-Aldrich, and the ZnO NPs with a diameter of 14 nm were purchased from PlasmaChem GmbH, Figure 1b. The nanocomposite thin film was
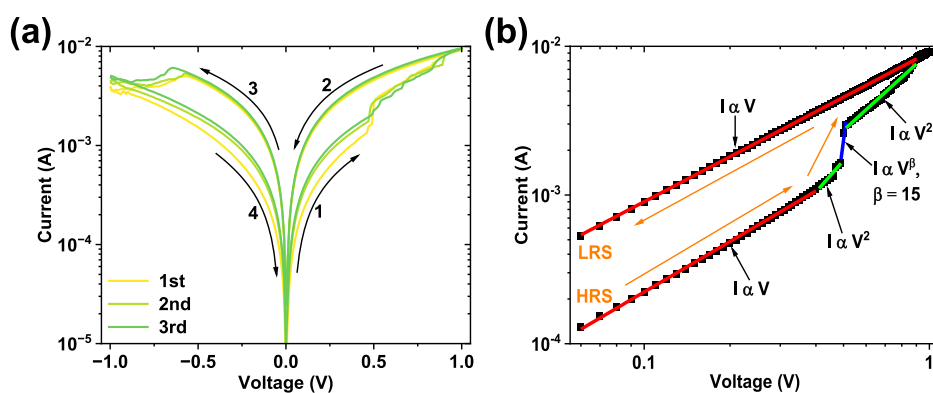
Figure 3. (a) $I-V$ characteristics for a device with $R_m = 0.1$ exhibiting bipolar resistive switching. The device switches from a HRS to a LRS under positive bias, maintaining this state until a negative bias causes a transition back to the HRS. (b) $\log(I)-\log(V)$ curve for the ZnO NPs–PDR1A device under positive bias, demonstrating the conduction mechanism of SCLC.

made by mixing PDR1A with ZnO NPs and depositing this solution *via* a spin-coating process (1000 rpm for 30 s). The spincoatable solution of PDR1A and ZnO NPs was made by mixing a solution of PDR1A in tetrahydrofuran (5% weight/weight) with a solution of ZnO NPs in toluene (1% weight/weight). The volume of the ZnO NP solution was varied to give ZnO NPs–PDR1A nanocomposite films with a different mass ratio (R_m) of the ZnO NPs, that is, 0.005, 0.01, 0.03, 0.05, 0.07, and 0.1 wt %, in PDR1A. The thin film was annealed at ~95 °C for 8 h to remove unwanted solvent. A 200 nm thick Au top electrode was deposited by a thermal evaporation process through a shadow mask. The $I-V$ sweeps were carried out using a probe station equipped with an HP4140B source-meter unit. Photomechanical expansion/contraction of the ZnO NPs–PDR1A film was induced by irradiation with either circularly or linearly polarized light generated from an argon ion laser tuned to a wavelength of 514 nm. The spot size of the laser beam had a diameter of 3 mm, and the average power per unit area for the exposed device was 180 mW cm^{-2}.

3. RESULTS AND DISCUSSION

The electronic switching properties of the devices with different mass concentrations (R_m) of ZnO NPs in PDR1A were studied. The $I-V$ characteristics of the devices in a semilogarithmic plot are shown in Figure 2a. In addition, the conductance of each device as a function of mass concentration, Figure 2b, is determined by averaging the measured current in the Ohmic region of the $I-V$ plot, over five consecutive $I-V$ sweeps. The plot shows that a large increase in the device conductance, up to 3 orders of magnitude, occurs at a threshold $R_m = 0.05\%$. While the devices with different concentrations all show some hysteresis, devices below this threshold have a low separation between resistance states and generally suffer from instability, leading to a lack of reproducibility. For concentrations of 0.05–0.1 wt % ZnO NPs, the devices showed reproducible resistive switching behavior over consecutive cycles. Interestingly, a previously reported result,[40] which investigated concentrations of 2, 5, and 10 wt % ZnO NPs, found that devices of 2 wt % ZnO NPs showed better stability and more reproducible memory switching than the very high concentration of 5 and 10 wt % ZnO NPs. Thus, in general, there seems to be an optimal concentration of approximately 0.05–2 wt % for achieving the best memory performance.

As the electronic characteristics of the devices are strongly dependent on the ZnO NP concentration, we suspect the NP morphology is like that observed previously for metal Au NPs embedded in PDR1A, whereby annealing of the polymer

during fabrication causes migration of the NPs to surface defect sites.[19] This creates an inhomogeneous percolation threshold in the device conductance *versus* NP concentration relationship that is caused by the NPs forming conducting pathways between top and bottom electrodes. This formation of inhomogeneous percolating conducting pathways leads to a sharp increase in the device conductance even at very low NP volume fraction, much lower than the normal percolation threshold observed in 3D homogeneous systems with spherical fillers, being found experimentally[41] to be ≈20%. This is similarly present in this system, where a large increase in conductance occurs above concentrations of $R_m \sim 0.03\%$, as shown in Figure 2b. The presence of these conducting pathways was also observed to affect the memristor switching. Similarly, in this system, the ON and OFF currents and ON/OFF ratio can be controlled by changing the ZnO NP concentration in PDR1A, as shown in Figure 2c. The plot shows the ON and OFF currents increase upon increasing the ZnO NP concentration. The plot also shows that the maximum ON/OFF ratio was achieved at $R_m = 0.03\%$. These results are in good agreement with the results reported previously for devices consisting of ZnO NPs embedded within the polymethyl methacrylate.[42]

Figure 3a shows three successive $I-V$ sweeps carried out on a device with $R_m = 0.1\%$. The direction of current sweeps is indicated by arrows. The device is initially in a high resistance state (HRS) and could be switched to a low resistance state (LRS) using a positive DC sweep from 0 to 1 V. Under positive bias, a sudden increase of the current (SET process) was observed consistently at ~0.5 V. The device could be switched back to the HRS (RESET process) by the application of a negative bias of ~−0.75 V, representing a typical bipolar switching behavior (first sweep). Subsequent $I-V$ sweeps (second and third sweeps) are like the initial sweep, indicating that no electroforming process is required to initialize the devices for the resistive switching effect. This repeatable bipolar switching achieved at low voltages with good separation between the resistance states is a desirable property for low power consumption memory applications.

The conduction mechanism in our device is examined by plotting the positive part of the $I-V$ sweep on a log–log scale, as shown in Figure 3b. The fit suggests that the conduction mechanism in our device is dominated by the space-charge-limited current (SCLC) model. Initially, from 0.0 to 0.4 V with the device in the HRS, the device shows a linear dependence of

current with applied voltage ($I \propto V$), with a slope of ≈1. This is attributed to the Ohmic conduction mechanism, which arises from thermally generated charge carriers.[20] At higher potential, $0.41 \leq V \leq 0.49$ V, the slope changes to ≈2, and the current shows the voltage square dependence ($I \propto V^2$). In this region, charge injection from the electrode begins to dominate, and trap-controlled SCLC occurs, as described using the Mott−Gurney law[43]

$$J = \frac{9\varepsilon\mu V^2}{8d^3}$$

(1)

where J is the current density, ε is the dielectric constant, μ is the free carrier mobility, V is the applied voltage, and d is the insulator thickness. At a threshold of 0.5 V, a much steeper rate of current increase occurs ($I \propto V^\beta$, $\beta \approx 15$). This indicates that all traps are filled, and the conduction mechanism in this region thereafter can be ascribed to trap-filled SCLC. In the region of $0.51 \leq V \leq 1$ V, the device switches from the HRS to the LRS with a voltage square dependence ($I \propto V^2$). In the case of the LRS and the return of the applied voltage back to 0 V, the conduction mechanism is dominated by Ohmic conduction, featuring the linear dependence of current with applied voltage, $I \propto V$. A similar conduction mechanism was previously observed in ZnO NPs/polymer nanocomposites.[28,44]

The operating mechanism of the SET and RESET processes for the ZnO NPs−PDR1A nanocomposite-based devices is proposed. Figure 4 shows a schematic diagram of the
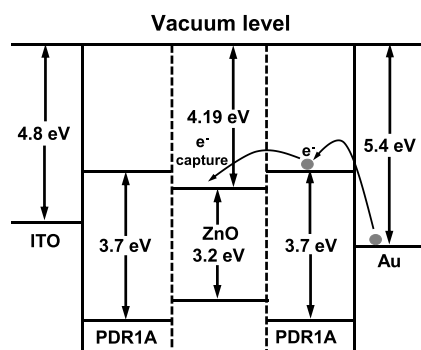

Figure 4. Schematic diagram of the energy levels for the ITO/ZnO NPs−PDR1A/Au device.

electronic structure for the ITO/ZnO NPs−PDR1A/Au device under a positive voltage polarity, where the ITO electrode is positive with respect to Au. The LUMO and HOMO represent the energy levels of the lowest unoccupied molecular orbital and the highest occupied molecular orbital of the PDR1A film, respectively. The energy levels for ZnO NPs are taken from ref 45 and those for PDR1A are taken from ref 46. A relatively large barrier is expected for hole injection from the ITO electrode into the HOMO level of the PDR1A. The energy gap between the HOMO and LUMO levels of PDR1A is estimated to be ∼3.7 eV,[46] but their position with respect to the work function of the metal is not currently known. The wide band gap of the PDR1A film and the very low current observed in devices containing only PDR1A (i.e., no NPs) indicates that PDR1A in its pure state is a good insulating material. Upon application of a positive voltage on the ITO electrode, electrons are initially injected from the Au electrode into the LUMO level of PDR1A via thermally generated

carriers. Increasing the applied voltage gradually increases the injection process via the SCLC, but in this case, injected electrons begin to be trapped by the ZnO NP trapping sites. Below the SET voltage, the device is still in the OFF state since some of the trapped electrons are transferred from the ZnO NPs to the ITO electrode, leaving the ZnO NPs partially occupied. Once the ZnO NP trap sites are fully occupied, as shown by the sharp increase in current with $I \propto V^\beta$, the device switches to the ON state at a SET voltage of 0.5 V. Thereafter, the I−V characteristics take on the trap-free SCLC behavior, as shown in Figure 3b, where $I \propto V^2$ over the range of $V = 0.5$−1.0 V. However, when the voltage is switched to negative bias conditions, the trapped electrons are gradually released, resulting in switching the device to the OFF state at a RESET voltage of $V \sim -0.75$ V.

A type of bipolar resistive switching effect has also been reported in a ZnO-based composite system, whereby ZnO particles[47] and ZnO microwires[48] were embedded in a methacrylic resin bisphenol-A-ethoxylate dimethacrylate (BEMA). The switching mechanism in these composite systems was attributed to interfacial chemistry at the boundary between the ZnO particles and ether-oxygens of ethylene glycol chains of the polymer, promoting an electron transfer between ZnO oxygen vacancies and the polymer matrix. However, unlike our above results, ideal memristor behavior was not observed since the current−voltage properties do not exhibit a pinched hysteresis curve at the origin. Rather, a capacitive type of the switching effect is observed, whereby the current−voltage curves do not crossover at any voltage in the sweep, or the curves crossover but not at $V = 0$. In both of these cases, the device is in a capacitive-like charged state at $V = 0$, and the device switching may instead be volatile in its operation. The current−voltage properties altogether indicate a very different type of switching mechanism in the BEMA polymer devices, which as indicated by the authors may instead be due to an electric field-induced interfacial exchange chemical reaction mechanism.

To characterize the optoelectronic response, DC sweeps were applied to an ITO/ZnO NPs−PDR1A/Au device at $R_m = 0.05\%$ to characterize the optoelectronic effect before and after illumination, as shown in Figure 5a. Initially, before illumination (black curve), the device showed a typical bipolar switching with SET and RESET processes occurring at positive and negative voltage polarities, respectively. Then, the device was illuminated by circularly polarized light for 30 min. This caused a shift in the I−V curve (red line indicates after expansion) to lower current, correlating with the photomechanical expansion of the polymer. Subsequent illumination with linearly polarized light for 15 min contracted the thickness of the polymer, resulting in a shift of the I−V curve (blue line indicates after contraction) back to its initial current state. Similarly, the effect can also be seen in the control device, which consists of only PDR1A, Figure 5b. The control device, incorporating the PDR1A film without ZnO NPs, exhibits very low conductivity, as expected for an insulating material, and no resistive switching effects are observed.

The modulation of device conductance upon illumination was also studied, as shown in Figure 5c. The plot shows that illumination of the control device with circularly polarized light (30 min) and linearly polarized light (15 min), which expands and contracts the thin film, respectively, results in changes of the device conductance of approximately 1 order of magnitude. We suspect that such a large change in the conductance is
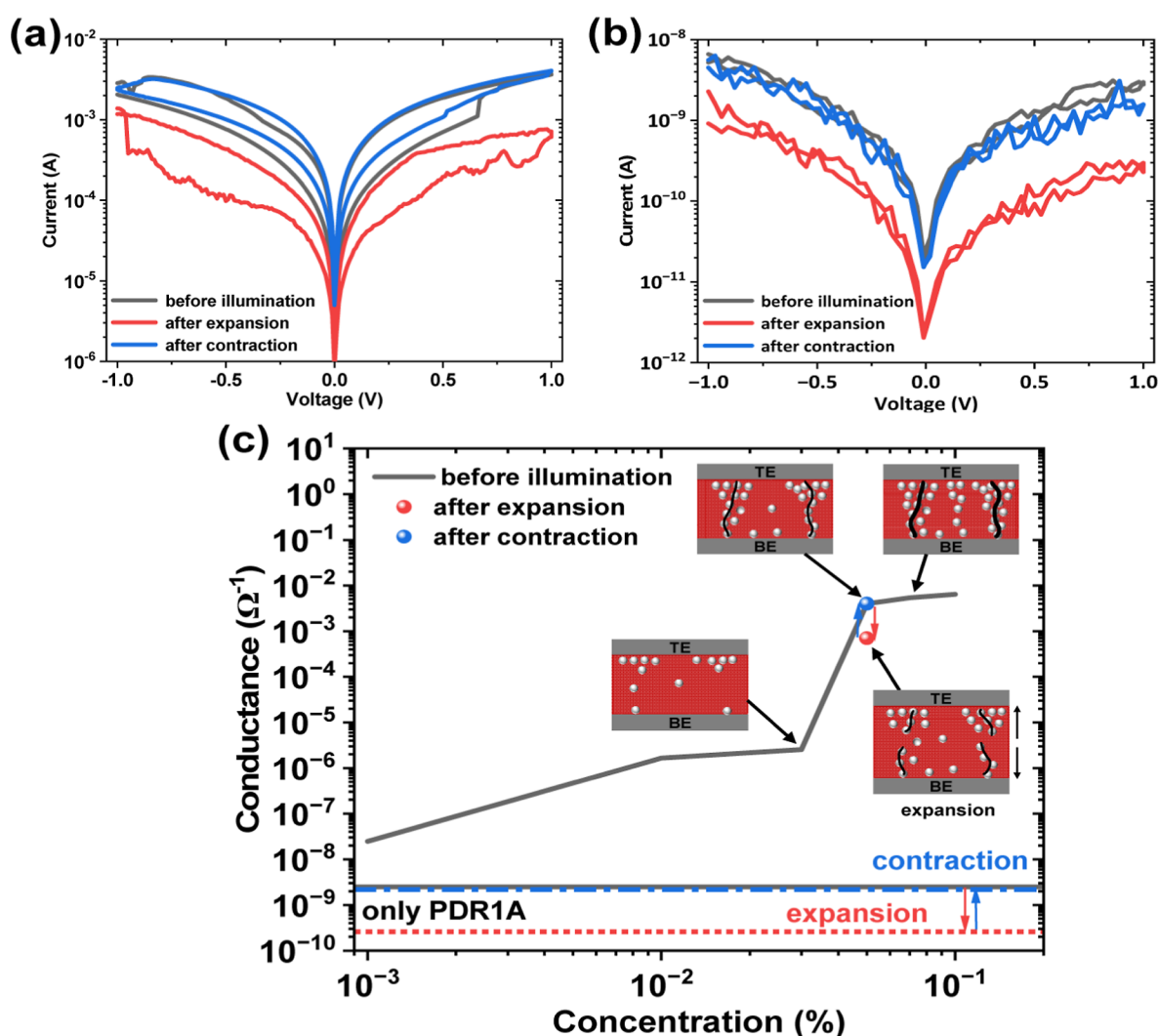
Figure 5. (a) $I-V$ characteristics of a device with $R_m = 0.05\%$ before and after illumination with circularly/linearly polarized light. Optically driven expansion/contraction of the polymer acts to modify both the HRS and LRS of the device, leading to a shift of the entire hysteresis curve. (b) $I-V$ characteristics for a control device, consisting of only PDR1A film without ZnO NPs, show a high resistance (small on and off currents) and only a minor change in this property after illumination and expansion of the PDR1A polymer film. (c) Conductance as a function of the concentration. The schematic insets show the formation of ZnO NP pathways below and above the threshold value ($R_m = 0.05\%$). Illumination with circularly polarized light expands the film and breaks the pathways, as a result changing the conductance as shown by the red and blue arrows. Modulation of the conductance of the PDR1A film containing no NPs is also shown by dashed lines following similar optical cycling.

caused by the breakage of the ZnO NP conducting pathways present in the device before illumination since the concentration of the device ($R_m = 0.05\%$) was specifically chosen to maximize this effect, as schematically presented in Figure 5c. As a result, the devices' conductance decreases 1 order of magnitude (red arrow shows the change in conductance). The change is reversible upon illumination with linearly polarized light for 15 min, shifting the device conductance back to its initial state (blue arrow). This demonstrates that the electronic properties of the device can be reversibly modified by optical means. The expansion and contraction of the polymer are driven by a molecular photochemical process known as trans–cis–trans isomerization. As this effect is common to many azo-containing polymers, future optical devices could be optimized to achieve larger OFF/ON resistance ratios, faster switching speeds, and increased stability by modifying the properties of the organic materials or the NP/polymer morphology.

We note here that the ZnO material generally exhibits photoconductive properties under UV illumination, which produces an increase in the conductivity of the material.[48] This effect is typically small in magnitude and opposite in sign to that observed in our devices, whereby the device conductance decreases upon optical irradiation because of the local increase in the thickness of the polymer layer. Previously, we have measured the photoconductance in ZnO devices that contain no PDR1A, and in this case, the change was less than 5% of that observed for devices containing both ZnO and PDR1A.[20] From this, we conclude that the photogeneration of trapped carriers does not play a dominant role in the operating properties of our ZnO NPs–PDR1A nanocomposite devices.

4. CONCLUSIONS

In summary, we demonstrate a polarization-dependent optoelectronic switching memory device made from a ZnO NP–PDR1A nanocomposite material. The device requires no forming process and displays bipolar resistive switching at low switching voltages. The device exhibits light-polarization-dependent changes in its resistive switching properties due to

the photoactive nature of the azobenzene moieties in PDR1A, which become preferentially aligned or misaligned depending on the polarization of incident light. The effect is reversible by the changing the polarization of the light. The fitting of the $I-V$ sweep showed that the conduction mechanism for the transition from the HRS to the LRS is dominated by SCLC, and the SET/RESET switching processes are governed by a trapping/de-trapping effect. This work suggests that the fabrication of a nanocomposite-based optical switching memory using a vacuum-free, low-cost, and fast spin-coating method could have a potential application for future optoelectronic devices.

■ AUTHOR INFORMATION

Corresponding Author

     Neil T. Kemp − *School of Physics and Astronomy, University of Nottingham, Nottingham NG7 2RD, U.K.;* ⊙ orcid.org/0000-0002-1906-4608; Email: Neil.Kemp@nottingham.ac.uk

Authors

     Ayoub H. Jaafar − *School of Physics and Astronomy, University of Nottingham, Nottingham NG7 2RD, U.K.;* ⊙ orcid.org/0000-0001-7305-4542

     Chris Lowe − *School of Mathematics and Physical Sciences, University of Hull, Hull HU6 7RX, U.K.*

     Alex Gee − *Department of Materials, University of Oxford, Oxford OX1 3PH, U.K.*

Complete contact information is available at:
https://pubs.acs.org/10.1021/acsapm.2c02034

Notes

The authors declare no competing financial interest.

■ ACKNOWLEDGMENTS

■ REFERENCES

(1) Pei, Y.; Li, Z.; Li, B.; Zhao, Y.; He, H.; Yan, L.; Li, X.; Wang, J.; Zhao, Z.; Sun, Y.; Zhou, Z.; Zhao, J.; Guo, R.; Chen, J.; Yan, X. A Multifunctional and Efficient Artificial Visual Perception Nervous System with Sb 2 Se 3 /CdS-Core/Shell (SC) Nanorod Arrays Optoelectronic Memristor. *Adv. Funct. Mater.* **2022**, *32*, 2203454.

(2) Zhou, F.; Zhou, Z.; Chen, J.; Choy, T. H.; Wang, J.; Zhang, N.; Lin, Z.; Yu, S.; Kang, J.; Wong, H. S. P.; Chai, Y. Optoelectronic Resistive Random Access Memory for Neuromorphic Vision Sensors. *Nat. Nanotechnol.* **2019**, *14*, 776−782.

(3) Tan, H.; Liu, G.; Zhu, X.; Yang, H.; Chen, B.; Chen, X.; Shang, J.; Lu, W. D.; Wu, Y.; Li, R. W. An Optoelectronic Resistive Switching Memory with Integrated Demodulating and Arithmetic Functions. *Adv. Mater.* **2015**, *27*, 2797−2803.

(4) Mao, J. Y.; Zhou, L.; Zhu, X.; Zhou, Y.; Han, S. T. Photonic Memristor for Future Computing: A Perspective. *Adv. Opt. Mater.* **2019**, *7*, 1900766.

(5) Chua, L. Memristor, Hodgkin-Huxley, and Edge of Chaos. *Nanotechnology* **2013**, *24*, 383001.

(6) He, H. K.; Yang, R.; Zhou, W.; Huang, H. M.; Xiong, J.; Gan, L.; Zhai, T. Y.; Guo, X. Photonic Potentiation and Electric Habituation in Ultrathin Memristive Synapses Based on Monolayer MoS2. *Small* **2018**, *14*, 1800079.

(7) Šuch, O.; Klimo, M.; Kemp, N. T.; Škvarek, O. Passive Memristor Synaptic Circuits with Multiple Timing Dependent Plasticity Mechanisms. *AEU-Int. J. Electron. Commun.* **2018**, *96*, 252−259.

(8) Zhai, Y.; Yang, X.; Wang, F.; Li, Z.; Ding, G.; Qiu, Z.; Wang, Y.; Zhou, Y.; Han, S. T. Infrared-Sensitive Memory Based on Direct-Grown MoS2 -Upconversion-Nanoparticle Heterostructure. *Adv. Mater.* **2018**, *30*, 1803563.

(9) Pei, Y.; Yan, L.; Wu, Z.; Lu, J.; Zhao, J.; Chen, J.; Liu, Q.; Yan, X. Artificial Visual Perception Nervous System Based on Low-Dimensional Material Photoelectric Memristors. *ACS Nano* **2021**, *15*, 17319−17326.

(10) Bogle, K.; Narwade, R.; Phatangare, A.; Dahiwale, S.; Mahabole, M.; Khairnar, R. Optically modulated resistive switching in BiFeO3thin film. *Phys. Status Solidi A* **2016**, *213*, 2183−2188.

(11) Huebner, C. F.; Tsyalkovsky, V.; Bandera, Y.; Burdette, M. K.; Shetzline, J. A.; Tonkin, C.; Creager, S. E.; Foulger, S. H. Nonvolatile Optically-Erased Colloidal Memristors. *Nanoscale* **2015**, *7*, 1270−1279.

(12) Emboras, A.; Goykhman, I.; Desiatov, B.; Mazurski, N.; Stern, L.; Shappir, J.; Levy, U. Nanoscale Plasmonic Memristor with Optical Readout Functionality. *Nano Lett.* **2013**, *13*, 6151−6155.

(13) He, K.; Liu, Y.; Yu, J.; Guo, X.; Wang, M.; Zhang, L.; Wan, C.; Wang, T.; Zhou, C.; Chen, X. Artificial Neural Pathway Based on a Memristor Synapse for Optically Mediated Motion Learning. *ACS Nano* **2022**, *16*, 9691−9700.

(14) Ungureanu, M.; Zazpe, R.; Golmar, F.; Stoliar, P.; Llopis, R.; Casanova, F.; Hueso, L. E. A Light-Controlled Resistive Switching Memory. *Adv. Mater.* **2012**, *24*, 2496−2500.

(15) Jaafar, A. H.; Kemp, N. T. Wavelength Dependent Light Tunable Resistive Switching Graphene Oxide Nonvolatile Memory Devices. *Carbon* **2019**, *153*, 81−88.

(16) Ling, H.; Tan, K.; Fang, Q.; Xu, X.; Chen, H.; Li, W.; Liu, Y.; Wang, L.; Yi, M.; Huang, R.; Qian, Y.; Xie, L.; Huang, W. Light-Tunable Nonvolatile Memory Characteristics in Photochromic RRAM. *Adv. Electron. Mater.* **2017**, *3*, 1900416.

(17) Mosciatti, T.; Bonacchi, S.; Gobbi, M.; Ferlauto, L.; Liscio, F.; Giorgini, L.; Orgiu, E.; Samorì, P. Optical Input/Electrical Output Memory Elements Based on a Liquid Crystalline Azobenzene Polymer. *ACS Appl. Mater. Interfaces* **2016**, *8*, 6563−6569.

(18) Chen, X.; Zhu, X.; Zhang, S. R.; Pan, J.; Huang, P.; Zhang, C.; Ding, G.; Zhou, Y.; Zhou, K.; Roy, V. A. L.; Han, S. T. Controlled Nonvolatile Transition in Polyoxometalates-Graphene Oxide Hybrid Memristive Devices. *Adv. Mater. Technol.* **2019**, *4*, 1800551.

(19) Jaafar, A. H.; O'Neill, M.; Kelly, S. M.; Verrelli, E.; Kemp, N. T. Percolation Threshold Enables Optical Resistive-Memory Switching and Light-Tuneable Synaptic Learning in Segregated Nanocomposites. *Adv. Electron. Mater.* **2019**, *5*, 1900197.

(20) Jaafar, A. H.; Gray, R. J.; Verrelli, E.; O'Neill, M.; Kelly, S. M.; Kemp, N. T. Reversible Optical Switching Memristors with Tunable STDP Synaptic Plasticity: A Route to Hierarchical Control in Artificial Intelligent Systems. *Nanoscale* **2017**, *9*, 17091−17098.

(21) Kossifos, K. M.; Antoniades, M. A.; Georgiou, J.; Jaafar, A. H.; Kemp, N. T. An Optically-Programmable Absorbing Metasurface. *IEEE International Symposium on Circuits and Systems (ISCAS)*; IEEE: Florence, Italy, 2018.

(22) Jaafar, A. H.; Al Chawa, M. M.; Cheng, F.; Kelly, S. M.; Picos, R.; Tetzlaff, R.; Kemp, N. T. Polymer/TiO2Nanorod Nanocomposite Optical Memristor Device. *J. Phys. Chem. C* **2021**, *125*, 14965−14973.

(23) Verrelli, E.; Gray, R. J.; O'Neill, M.; Kelly, S. M.; Kemp, N. T. Microwave Oven Fabricated Hybrid Memristor Devices for Non-Volatile Memory Storage. *Mater. Res. Express* **2014**, *1*, 046305.

(24) Rajan, K.; Chiappone, A.; Perrone, D.; Bocchini, S.; Roppolo, I.; Bejtka, K.; Castellino, M.; Pirri, C. F.; Ricciardi, C.; Chiolerio, A. Ionic Liquid-Enhanced Soft Resistive Switching Devices. *RSC Adv.* **2016**, *6*, 94128−94138.

(25) Rajan, K.; Bocchini, S.; Chiappone, A.; Roppolo, I.; Perrone, D.; Bejtka, K.; Ricciardi, C.; Pirri, C. F.; Chiolerio, A. Spin-Coated Silver Nanocomposite Resistive Switching Devices. *Microelectron. Eng.* **2017**, *168*, 27−31.

(26) Gray, R. J.; Jaafar, A. H.; Verrelli, E.; Kemp, N. T. Method to Reduce the Formation of Crystallites in ZnO Nanorod Thin-Films Grown via Ultra-Fast Microwave Heating. *Thin Solid Films* **2018**, *662*, 116−122.

(27) Jaafar, A. H.; Gee, A.; Hamza, A. O.; Eling, C. J.; Bouillard, J.-S. G.; Adawi, A. M.; Kemp, N. T. Evidence of Nanoparticle Migration in Polymeric Hybrid Memristor Devices. *2020 European Conference on Circuit Theory and Design (ECCTD)*; IEEE, 2020; pp 1−4.

(28) Jaafar, A. H.; Gee, A.; Kemp, N. T. Nanorods Versus Nanoparticles: A Comparison Study of Au/ZnO-PMMA/Au Non-Volatile Memory Devices Showing the Importance of Nanostructure Geometry on Conduction Mechanisms and Switching Properties. *IEEE Trans. Nanotechnol.* **2020**, *19*, 236−246.

(29) Lee, C.-T.; Yu, L.-Z.; Chen, H.-C. Memory Bistable Mechanisms of Organic Memory Devices. *Appl. Phys. Lett.* **2010**, *97*, 043301.

(30) Zhao, J. H.; Thomson, D. J.; Pillai, R. G.; Freund, M. S. Dynamic Resistive Crossbar Memory Based on Conjugated Polymer Composite. *Appl. Phys. Lett.* **2009**, *94*, 092113.

(31) Gu, C.; Lee, J. S. Flexible Hybrid Organic-Inorganic Perovskite Memory. *ACS Nano* **2016**, *10*, 5413−5418.

(32) Choi, J.; Park, S.; Lee, J.; Hong, K.; Kim, D. H.; Moon, C. W.; do Park, G.; Suh, J.; Hwang, J.; Kim, S. Y.; Jung, H. S.; Park, N. G.; Han, S.; Nam, K. T.; Jang, H. W. Organolead Halide Perovskites for Low Operating Voltage Multilevel Resistive Switching. *Adv. Mater.* **2016**, *28*, 6562−6567.

(33) Seo, J. Y.; Choi, J.; Kim, H. S.; Kim, J.; Yang, J. M.; Cuhadar, C.; Han, J. S.; Kim, S. J.; Lee, D.; Jang, H. W.; Park, N. G. Wafer-Scale Reliable Switching Memory Based on 2-Dimensional Layered Organic-Inorganic Halide Perovskite. *Nanoscale* **2017**, *9*, 15278−15285.

(34) Ribierre, J. C.; Aoyama, T.; Muto, T.; André, P. Hybrid Organic-Inorganic Liquid Bistable Memory Devices. *Org. Electron.* **2011**, *12*, 1800−1805.

(35) Han, J. S.; van Le, Q.; Choi, J.; Hong, K.; Moon, C. W.; Kim, T. L.; Kim, H.; Kim, S. Y.; Jang, H. W. Air-Stable Cesium Lead Iodide Perovskite for Ultra-Low Operating Voltage Resistive Switching. *Adv. Funct. Mater.* **2018**, *28*, 1705783.

(36) Natansohn, A.; Rochon, P. Photoinduced Motions in Azo-Containing Polymers. *Chem. Rev.* **2002**, *102*, 4139−4176.

(37) Tanchak, O. M.; Barrett, C. J. Light-Induced Reversible Volume Changes in Thin Films of Azo Polymers: The Photo-mechanical Effect. *Macromolecules* **2005**, *38*, 10566−10570.

(38) Karageorgiev, P.; Neher, D.; Schulz, B.; Stiller, B.; Pietsch, U.; Giersig, M.; Brehmer, L. From Anisotropic Photo-Fluidity towards Nanomanipulation in the Optical near-Field. *Nat. Mater.* **2005**, *4*, 699−703.

(39) Lee, S.; Kang, H. S.; Park, J. K. Directional Photofluidization Lithography: Micro/Nanostructural Evolution by Photofluidic Motions of Azobenzene Materials. *Adv. Mater.* **2012**, *24*, 2069−2103.

(40) Zhao, E.; Liu, D.; Liu, L.; Yang, X.; Kan, W.; Sun, Y. Unipolar Nonvolatile Memory Devices Based on the Composites of Poly(9-Vinylcarbazole) and Zinc Oxide Nanoparticles. *J. Mater. Sci.: Mater. Electron.* **2017**, *28*, 11749−11754.

(41) Powell, M. J. Site percolation in randomly packed spheres. *Phys. Rev. B: Condens. Matter Mater. Phys.* **1979**, *20*, 4194−4198.

(42) Thanh Dao, T.; Viet Tran, T.; Higashimine, K.; Okada, H.; Mott, D.; Maenosono, S.; Murata, H. High-Performance Nonvolatile Write-Once-Read-Many-Times Memory Devices with ZnO Nano-particles Embedded in Polymethylmethacrylate. *Appl. Phys. Lett.* **2011**, *99*, 233303.

(43) Chiu, F.-C. Review Article A Review on Conduction Mechanisms in Dielectric Films. *Adv. Mater. Sci. Eng.* **2014**, *2014*, 578168.

(44) Son, D.; Park, D.; Choi, W. K.; Cho, S.; Kim, W.; Kim, T. W. Carrier transport in flexible organic bistable devices of ZnO nanoparticles embedded in an insulating poly(methyl methacrylate) polymer layer. *Nanotechnology* **2009**, *20*, 195203−195209.

(45) Lin, J. M.; Lin, H. Y.; Cheng, C. L.; Chen, Y. F. Giant Enhancement of Bandgap Emission of ZnO Nanorods by Platinum Nanoparticles. *Nanotechnology* **2006**, *17*, 4391−4394.

(46) Poprawa-Smoluch, M.; Baggerman, J.; Zhang, H.; Maas, H. P. A.; De Cola, L.; Brouwer, A. M. Photoisomerization of Disperse Red 1 Studied with Transient Absorption Spectroscopy and Quantum Chemical Calculations. *J. Phys. Chem. A* **2006**, *110*, 11926−11937.

(47) Chiolerio, A.; Roppolo, I.; Bejtka, K.; Asvarov, A.; Pirri, C. F. Resistive Hysteresis in Flexible Nanocomposites and Colloidal Suspensions: Interfacial Coupling Mechanism Unveiled. *RSC Adv.* **2016**, *6*, 56661−56667.

(48) Chiolerio, A.; Roppolo, I.; Cauda, V.; Crepaldi, M.; Bocchini, S.; Bejtka, K.; Verna, A.; Pirri, C. F. Ultraviolet Mem-Sensors: Flexible Anisotropic Composites Featuring Giant Photocurrent Enhancement. *Nano Res.* **2015**, *8*, 1956−1963.

📖 Recommended by ACS

Double-Network Protein Hydrogels as Flexible Pressure Sensors for Contactless Delivery

Anbo Zheng, Yanxu Chen, *et al.*
MARCH 03, 2023
ACS APPLIED POLYMER MATERIALS   READ 🔗

Shape Memory Polymer Constructed by π−π Stacking with Ultrafast Photoresponse and Self-Healing Performance

Jiaye Dai, Xuan Zhang, *et al.*
MARCH 06, 2023
ACS APPLIED POLYMER MATERIALS   READ 🔗

A Bioinspired Surface with Synergistic Effect of Anisotropy and Gradient Microstructures for Controllable Fluid Transportation

Kai Sheng, Xiwei Wang, *et al.*
MARCH 03, 2023
ACS APPLIED POLYMER MATERIALS   READ 🔗

Molecular Weight Distribution Shape Dependence of the Crystallization Kinetics of Semicrystalline Polymers Based on Linear Unimodal and Bimodal Polyethylenes

Chuanjiang Long, Zhong-Ren Chen, *et al.*
MARCH 02, 2023
ACS APPLIED POLYMER MATERIALS   READ 🔗

Get More Suggestions >